

The Bayesian Context Trees State Space Model: Interpretable mixture models for time series

Ioannis Papageorgiou ^{*} Ioannis Kontoyiannis [†]

May 23, 2022

Abstract

A general hierarchical Bayesian framework is introduced for mixture modelling of real-valued time series, including a collection of effective tools for learning and inference. At the top level, a *discrete* context (or ‘state’) is extracted for each sample, consisting of a discretised version of some of the most recent observations preceding it. The set of all relevant contexts are represented as a discrete context tree. At the bottom level, a different *real-valued* time series model is associated with each context (i.e., with each state). This defines a very general framework that can be used in conjunction with any existing model class to build flexible and *interpretable* mixture models. We introduce algorithms that allow for efficient, *exact* Bayesian inference; in particular, the maximum *a posteriori* probability (MAP) model, including the relevant MAP context tree, can be identified exactly. These algorithms can be updated sequentially, facilitating efficient online forecasting. The utility of the general framework is illustrated in detail when autoregressive (AR) models are used at the bottom level, resulting in a nonlinear AR mixture model. Our methods are found to outperform several state-of-the-art techniques on both simulated and real-world data from economics and finance, both in terms of forecasting accuracy and computational requirements.

Keywords. Time series, Interpretable mixture models, Exact Bayesian inference, Forecasting, State space models, Autoregressive models, Context trees.

^{*}Department of Engineering, University of Cambridge, Trumpington Street, Cambridge CB2 1PZ, UK. Email: ip307@cam.ac.uk.

[†]Statistical Laboratory, Centre for Mathematical Sciences, University of Cambridge, Wilberforce Road, Cambridge CB3 0WB, UK. Email: yiannis@maths.cam.ac.uk.

1 Introduction

Time series modelling, inference and forecasting are critical tasks in statistics and machine learning (ML), with important applications throughout the sciences and engineering. A wide range of approaches exist, including classical statistical methods [10, 29, 19, 33] as well as modern ML techniques, notably matrix factorisations [87, 21], Gaussian processes (GP) [61, 66, 23], and neural networks [7, 3, 88]. Despite their popularity, there has not been conclusive evidence that in general the latter outperform the former in the time series setting [50, 49, 1]. Motivated in part by the two well-known limitations of neural network models (see, e.g., [7]), namely, the lack of interpretability and data efficiency, in this work we propose a general class of flexible hierarchical Bayesian models, which are both naturally *interpretable* and suitable for applications with limited training data. Also, we provide computationally efficient – linear complexity – algorithms for inference and prediction, offering another practical advantage compared to standard ML methods which have greater computational requirements due to the heavier training involved [50].

Roughly speaking, time series models can be broadly categorised in two classes, depending on the absence or presence of an underlying hidden state process. The first class includes the family of autoregressive (AR) and autoregressive integrated moving average (ARIMA) models along with their extensions and generalisations, which directly model the mapping from previous to current observations. Besides the classical AR and ARIMA models [10, 76, 73], nonlinear AR models have been proposed, using both GPs [66, 27, 11, 78, 53] and neural networks to model nonlinear dynamics. Feed-forward neural networks have been used since the 90s in this setting [88], as in the Neural Network AR (NNAR) model. More recently, recurrent neural networks (RNN) have also been employed [28, 69, 54], with the DeepAR model of [69] that uses Long Short-Term Memory (LSTM) cells [31] being one of the most successful approaches.

The second class consists of State Space Models (SSM) [19, 33], which can describe more complex dynamics by allowing an underlying hidden state process (state-transition) together with an observation model (emission). Classical approaches here include the linear Gaussian SSM, for which the Kalman filter [37] can be used for inference, and exponential smoothing methods; see [33] for a detailed review. Again, various extensions have been proposed by making the transition and/or emission equations nonlinear, using both GPs [77, 25, 24, 20, 78] and neural networks [45, 44, 89, 38, 59, 16]. However, inference in these settings becomes a quite challenging task, requiring sophisticated and computationally-intense approximate techniques, including Particle MCMC [18, 6] and variational methods like stochastic gradient variational Bayes (SGVB) [40, 62].

In this work, we introduce an intermediate Bayesian modelling approach that combines important features of both the above classes: We first identify meaningful discrete states, but these are *observable* rather than hidden, and given by the discretised values of some of the most recent samples. Then we associate a different time series model with each of these discrete *context-based states*. In technical terms, we define a hierarchical Bayesian model, which at the top level selects the set of relevant states (that can be viewed as providing an adaptive partition of the state space), and at the bottom level associates an arbitrary time series model to each state. These collections of states (equivalently, the corresponding state space partitions) are naturally represented as discrete *context-tree* models [42], which are shown to admit a natural *interpretation* and to enable capturing important aspects of the structure present in the data. We refer to the resulting model class as the *Bayesian Context Trees State Space Model* (BCT-SSM).

Although we refer to the BCT-SSM as a ‘model’, it is in fact a general framework for building Bayesian mixture models for time series, that can be used in conjunction with any existing model class. The resulting model family is rich, flexible, and much more general than the class one starts with. For example, using any of the standard linear families (like the classical AR or ARIMA) leads to much more general models that can in fact capture highly nonlinear trends in the data, and are also easily interpretable. We show that in addition to resulting in the construction of flexible model classes, employing this particular type of observable state process (as opposed to a conventional hidden state process) also makes it possible to perform effective Bayesian inference. This is achieved by exploiting the structure of context-tree models and by extending the algorithms of [42, 57], which were previously used only in the restricted setting of discrete-valued time series.

These tools make the BCT-SSM a powerful Bayesian framework that allows for *exact* and computationally very efficient Bayesian inference. In particular, the *evidence* [48] can be computed exactly, with all models and parameters integrated out. Furthermore, the *a posteriori* most likely (MAP) partition (i.e., the MAP set of discrete states) can be identified, along with its exact posterior probability. Following the Bayesian approach here is particularly important, as it means that the data automatically select the set of relevant states. In contrast, maximum likelihood would overfit and select a large number of irrelevant states, with consequences both in the interpretation and the out-of-sample prediction performance of the fitted model. Finally, it is shown that our algorithms allow for efficient sequential updates, which are ideally suited for online forecasting, and provide an important practical advantage compared to standard ML time series approaches.

To illustrate the application of the general framework, we study in detail the case where AR models are used as building blocks for the BCT-SSM, with a different AR model associated to each discrete state. We refer to the resulting model class as the *Bayesian context tree autoregressive* (BCT-AR) model; it is shown to be a flexible, nonlinear mixture of AR models that generalises popular AR mixtures, including the threshold AR (TAR) models [74, 75, 73] and the mixture AR (MAR) models of [83]. The BCT-AR model is found to outperform several state-of-the-art methods in simulated experiments and standard applications of nonlinear time series from economics and finance, both in terms of forecasting accuracy and computational requirements.

Finally, we note that a number of earlier approaches employ discrete patterns in the analysis of real-valued time series [4, 5, 8, 26, 32, 47, 55, 68]. These works illustrate the fact that useful and meaningful information can indeed be extracted from discrete contexts. However, in most cases the methods are either application- or task-specific, and typically resort to *ad hoc* considerations for performing inference. In contrast, in this work discrete contexts are used in a natural manner, by defining a hierarchical Bayesian modelling structure upon which principled Bayesian inference is performed.

2 The Bayesian Context Trees State Space Model

2.1 Discrete contexts

A key element of our development is the use of an *observable* state for each sample x_n , based on discretised versions of some of the samples $(\dots, x_{n-2}, x_{n-1})$ preceding it. We refer to the string consisting of these discretised previous samples as the *discrete context*; it plays the role of a discrete-valued feature vector that can be used to identify additional useful structure in the

data. In order to extract these contexts, we consider simple piecewise constant quantisers from \mathbb{R} to a finite alphabet $A = \{0, 1, \dots, m - 1\}$, of the form,

$$Q(x) = \begin{cases} 0, & x < c_1, \\ i, & c_i \leq x \leq c_{i+1}, \quad 1 \leq i \leq m - 2, \\ m - 1, & x > c_{m-1}, \end{cases} \quad (1)$$

where, throughout this section, the thresholds $\{c_1, \dots, c_{m-1}\}$ and the resulting quantiser Q are considered fixed. A systematic way to infer the thresholds from data is described in Section 3.2.

We note that this general framework can be used in conjunction with an arbitrary way of extracting discrete features, based on an arbitrary mapping to a discrete alphabet, not necessarily of the form in (1). However, the quantisation needs to be meaningful in order to lead to useful results. Quantisers as in (1) offer a generally reasonable choice although, depending on the application at hand, there are other useful approaches, e.g., quantising percentage differences between successive samples.

2.2 Context trees

Given a quantiser Q with m levels as above, a maximum context length $D \geq 0$, and a proper m -ary context tree T , the context (or ‘state’) of each sample x_n is obtained as follows. Let $t = (Q(x_{n-1}), \dots, Q(x_{n-D}))$ be the discretised string of length D preceding x_n ; the *context* s of x_n is the unique leaf of T that is a suffix of t . For example, for the context tree of Figure 1, if $Q(x_{n-1}) = 0$ and $Q(x_{n-2}) = 1$ then $s = 01$, whereas if $Q(x_{n-1}) = Q(x_{n-2}) = 1$ then $s = 1$. The leaves of the tree define the set of discrete states in our hierarchical model. So, for the example BCT-SSM of Figure 1, the set of states is $\mathcal{S} = \{1, 01, 00\}$. Equivalently, this process can be viewed as defining a partition of \mathbb{R}^2 into three regions indexed by the contexts \mathcal{S} in T . [A tree T is *proper* if any node in T that is not a leaf has exactly m children. This means that for any string $t = (Q(x_{n-1}), \dots, Q(x_{n-D}))$ there is always a unique context s that is a leaf of T . Equivalently, proper trees define proper partitions, so that the resulting state space regions are disjoint and their union is the whole space \mathbb{R}^D .]

To complete the specification of the BCT-SSM, we need to associate a different time series model \mathcal{M}_s to each leaf s of the context tree T , giving a different conditional density for x_n . At time n , given the context s determined by the past D samples $(x_{n-1}, \dots, x_{n-D})$, the distribution of x_n is given by the model \mathcal{M}_s assigned to s . Although general non-parametric models could also be used, for the rest of this paper we consider parametric models with parameters θ_s at each leaf s . Altogether, the BCT-SSM consists of an m -ary quantiser Q , a proper m -ary tree T that defines the set of discrete states, and a collection of parameter vectors θ_s for the parametric models at the leaves of T .

Identifying T with the collection of its leaves \mathcal{S} , and writing x_i^j for the segment $(x_i, x_{i+1}, \dots, x_j)$, the likelihood induced by the BCT-SSM is,

$$p(x|\theta, T) := p(x_1^n | T, \theta, x_{-D+1}^0) = \prod_{i=1}^n p(x_i | T, \theta, x_{-D+1}^{i-1}) = \prod_{s \in T} \prod_{i \in B_s} p(x_i | T, \theta_s, x_{-D+1}^{i-1}), \quad (2)$$

where B_s is the set of indices $i \in \{1, 2, \dots, n\}$ such that the context of x_i is s , and $\theta = \{\theta_s ; s \in T\}$.

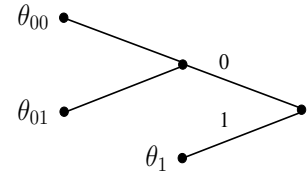


Figure 1: Example of a binary context tree T used for defining the set of discrete states-contexts

2.3 Bayesian modelling and inference

For the top level of the BCT-SSM, we consider collections of states represented by context trees T in the class $\mathcal{T}(D)$ [42] of all proper m -ary trees with depth no greater than D .

Prior structure. For the trees $T \in \mathcal{T}(D)$ with maximum depth $D \geq 0$ at the top level of the hierarchical model, we use the Bayesian Context Trees (BCT) prior of [42],

$$\pi(T) = \pi_D(T; \beta) = \alpha^{|T|-1} \beta^{|T|-L_D(T)}, \quad (3)$$

where $\beta \in (0, 1)$ is a hyperparameter, α is given by $\alpha = (1 - \beta)^{1/(m-1)}$, $|T|$ is the number of leaves of T , and $L_D(T)$ is the number of leaves of T at depth D . This prior penalises larger trees by an exponential amount, which is reasonable as it is naturally desirable to *a priori* penalise BCT-SSM models with large numbers of parameters to avoid overfitting. Given a tree model $T \in \mathcal{T}(D)$, we place an independent prior on each θ_s , so that $\pi(\theta|T) = \prod_{s \in T} \pi(\theta_s)$.

Typically, the main obstacle in performing Bayesian inference is the computation of the normalising constant $p(x)$ of the posterior (sometimes referred to as the *evidence*), in this case,

$$p(x) = \sum_{T \in \mathcal{T}(D)} \pi(T) p(x|T) = \sum_{T \in \mathcal{T}(D)} \pi(T) \int_{\theta} p(x|T, \theta) \pi(\theta|T) d\theta. \quad (4)$$

The power of the proposed Bayesian structure comes, in part, from the fact that, although $\mathcal{T}(D)$ is enormously rich, consisting of doubly-exponentially many models in D , it is actually possible to perform *exact* Bayesian inference efficiently. To that end, we introduce the Continuous Context Tree Weighting (CCTW) algorithm, and the Continuous Bayesian Context Tree (CBCT) algorithm, generalising the corresponding algorithms for discrete time series in [42]. It is shown that CCTW computes the normalising constant $p(x)$ exactly (Theorem 1), and CBCT identifies the MAP tree model (Theorem 2). In the Appendix we briefly discuss how the k -BCT algorithm of [42] can be similarly modified to obtain the top- k *a posteriori* most likely trees, but the details are omitted. The main difference from the discrete case in [42], both in the algorithmic descriptions and in the proofs of the theorems (given in the Appendix), is that we introduce a new generalised form of *estimated probabilities* that is needed in place of their simple discrete versions. These are given by,

$$P_e(s, x) = \int \prod_{i \in B_s} p(x_i | T, \theta_s, x_{-D+1}^{i-1}) \pi(\theta_s) d\theta_s. \quad (5)$$

Let $x = x_{-D+1}^n$ be a time series, and let $y_i = Q(x_i)$ denote the corresponding quantised samples.

CCTW: The continuous context-tree weighting algorithm

1. Build the tree T_{MAX} , whose leaves are all the discrete contexts y_{i-D}^{i-1} , $i = 1, 2, \dots, n$. Compute $P_e(s, x)$ as given in (5) for each node s of T_{MAX} .
2. Starting at the leaves and proceeding recursively towards the root compute:

$$P_{w,s} = \begin{cases} P_e(s, x), & \text{if } s \text{ is a leaf,} \\ \beta P_e(s, x) + (1 - \beta) \prod_{j=0}^{m-1} P_{w,sj}, & \text{otherwise,} \end{cases}$$

where s_j is the concatenation of context s and symbol j .

CBCT: The continuous Bayesian context tree algorithm

1. Build the tree T_{MAX} and compute $P_e(s, x)$ for each node s of T_{MAX} , as in CCTW.
2. Starting at the leaves and proceeding recursively towards the root compute:

$$P_{m,s} = \begin{cases} P_e(s, x), & \text{if } s \text{ is a leaf at depth } D, \\ \beta, & \text{if } s \text{ is a leaf at depth } < D, \\ \max \{ \beta P_e(s, x), (1 - \beta) \prod_{j=0}^{m-1} P_{m,sj} \}, & \text{otherwise.} \end{cases}$$

3. Starting at the root and proceeding recursively with its descendants, for each node s : If the maximum above is achieved by the first term, prune all its descendants from T_{MAX} .

Theorem 1. *The weighted probability $P_{w,s}$ at the root is exactly the normalising constant $p(x)$ of (4).*

Theorem 2. *For all $\beta \geq 1/2$, the tree T_1^* produced by the CBCT algorithm is the MAP tree model.*

Even in cases where the integrals in (5) are not tractable, the fact that they are in the form of standard marginal likelihoods makes it possible to compute them approximately using standard methods, e.g., [14, 15, 22, 86]. The above algorithms can then be used with these approximations as a way of performing approximate inference for the BCT-SSM. However, in this paper we do not investigate this further. Instead, we illustrate the general principle via an interesting example where the estimated probabilities can be computed explicitly and the resulting mixture model is a flexible nonlinear model of practical interest. This is described in the next section, where AR models \mathcal{M}_s are associated to each context s . We refer to the resulting model as the Bayesian context tree autoregressive (BCT-AR) model, which is just a particular instance of the general BCT-SSM.

2.4 Remarks: Discrete models for continuous data

Context-tree models were introduced as “tree sources” by Rissanen [63, 64, 65] in the 1980s in the information-theoretic literature, and they have been employed widely since then in connection with problems on *discrete* data. Tree source models were used with great success in the context of data compression [79, 81, 80], and more recently they have been found to be very effective in the analysis of discrete-valued time series within the Bayesian Context Trees (BCT) framework [42, 57, 56].

The central conceptual novelty of the present work is in showing that discrete context trees can in fact also be utilised in a very effective way for modelling *real-valued* time series, by representing meaningful context-based discrete states that are used to build flexible and interpretable mixture models of practical interest. We introduce a new construction for building context-dependent mixtures of models in any existing model class, combining a discrete context tree with an arbitrary existing family of *continuous* models. In fact, this is the first attempt of doing so, perhaps because at first glance context trees seem to be naturally suited only for discrete-valued data. An important step in the development of the BCT-SSM class is the introduction of a quantiser that extracts discrete contexts (Section 2.1), along with a principled Bayesian procedure for actually selecting an appropriate quantiser in practice (Section 3.2). Finally we are able to prove that, perhaps somewhat surprisingly, small modifications of the discrete BCT

algorithms of [42] can be used for exact inference in the much more general BCT-SSM setting (Section 2.3). The BCT-AR model described in the next section is new, as is the analysis of the estimated probabilities, the relevant posterior distributions, and the computational complexity of the CCTW and CBCT algorithms in this case.

3 The Bayesian context tree autoregressive model

Here we consider the BCT-SSM model class where an AR model of order p is associated to each leaf s of a context tree T , as,

$$x_n = \phi_{s,1}x_{n-1} + \cdots + \phi_{s,p}x_{n-p} + e_n = \boldsymbol{\phi}_s^\top \tilde{\mathbf{x}}_{n-1} + e_n, \quad e_n \sim \mathcal{N}(0, \sigma_s^2), \quad (6)$$

where $\boldsymbol{\phi}_s = (\phi_{s,1}, \dots, \phi_{s,p})^\top$ and $\tilde{\mathbf{x}}_{n-1} = (x_{n-1}, \dots, x_{n-p})^\top$.

The parameters of the model are the AR coefficients and the noise variance, so that $\theta_s = (\boldsymbol{\phi}_s, \sigma_s^2)$. We use an inverse-gamma prior for the noise variance, and a Gaussian prior for the AR coefficients, so that the joint prior on the parameters is $\pi(\theta_s) = \pi(\boldsymbol{\phi}_s | \sigma_s^2) \pi(\sigma_s^2)$, with,

$$\pi(\sigma_s^2) = \text{Inv-Gamma}(\tau, \lambda), \quad \pi(\boldsymbol{\phi}_s | \sigma_s^2) = \mathcal{N}(\boldsymbol{\mu}_o, \sigma_s^2 \boldsymbol{\Sigma}_o), \quad (7)$$

where $(\tau, \lambda, \boldsymbol{\mu}_o, \boldsymbol{\Sigma}_o)$ are the prior hyperparameters. This prior specification allows the exact computation of the estimated probabilities of (5), and also gives closed-form posteriors for the AR coefficients and the noise variance. These are given in Lemmas 1 and 2; their proofs are in Appendix B.

Lemma 1. *For the AR model, the estimated probabilities $P_e(s, x)$ as in (5) are given by,*

$$P_e(s, x) = C_s^{-1} \frac{\Gamma(\tau + |B_s|/2) \lambda^\tau}{\Gamma(\tau) (\lambda + D_s/2)^{\tau + |B_s|/2}}, \quad (8)$$

where $|B_s|$ is the cardinality of the set B_s in (2), i.e., the number of observations with context s , and,

$$C_s = \sqrt{(2\pi)^{|B_s|} \det(I + \boldsymbol{\Sigma}_o S_3)}, \quad D_s = s_1 + \boldsymbol{\mu}_o^\top \boldsymbol{\Sigma}_o^{-1} \boldsymbol{\mu}_o - (\mathbf{s}_2 + \boldsymbol{\Sigma}_o^{-1} \boldsymbol{\mu}_o)^\top (S_3 + \boldsymbol{\Sigma}_o^{-1})^{-1} (\mathbf{s}_2 + \boldsymbol{\Sigma}_o^{-1} \boldsymbol{\mu}_o),$$

with the sums s_1, \mathbf{s}_2, S_3 defined as:

$$s_1 = \sum_{i \in B_s} x_i^2, \quad \mathbf{s}_2 = \sum_{i \in B_s} x_i \tilde{\mathbf{x}}_{i-1}, \quad S_3 = \sum_{i \in B_s} \tilde{\mathbf{x}}_{i-1} \tilde{\mathbf{x}}_{i-1}^\top. \quad (9)$$

Lemma 2. *Given a tree model T , at each leaf s , the posterior distributions of the AR coefficients and the noise variance are given by,*

$$\pi(\sigma_s^2 | T, x) = \text{Inv-Gamma}(\tau + |B_s|/2, \lambda + D_s/2), \quad \pi(\boldsymbol{\phi}_s | T, x) = t_\nu(\mathbf{m}_s, P_s), \quad (10)$$

where t_ν denotes a multivariate t -distribution with ν degrees of freedom. Here, $\nu = 2\tau + |B_s|$, and,

$$\mathbf{m}_s = (S_3 + \boldsymbol{\Sigma}_o^{-1})^{-1} (\mathbf{s}_2 + \boldsymbol{\Sigma}_o^{-1} \boldsymbol{\mu}_o), \quad P_s^{-1} = \frac{2\tau + |B_s|}{2\lambda + D_s} (S_3 + \boldsymbol{\Sigma}_o^{-1}). \quad (11)$$

Corollary. *The MAP estimators of $\boldsymbol{\phi}_s$ and σ_s^2 are given, respectively, by,*

$$\widehat{\boldsymbol{\phi}}_s^{\text{MAP}} = \mathbf{m}_s, \quad \widehat{\sigma}_s^2^{\text{MAP}} = (2\lambda + D_s) / (2\tau + |B_s| + 2). \quad (12)$$

3.1 Computational complexity and sequential updates

For a time series x_1^n , with an initial segment x_{-D+1}^0 , the tree T_{MAX} in the CCTW algorithm has no more than $nD + 1$ nodes. For each symbol x_i in x_1^n , exactly $D + 1$ nodes of T_{MAX} need to be updated, corresponding to its contexts of length $0, 1, \dots, D$. For each one of these nodes, only the quantities $\{|B_s|, s_1, s_2, S_3\}$ need to be updated, which can be done efficiently by just adding an extra term to each sum. Using these and Lemma 1, the estimated probabilities $P_e(s, x)$ can be computed for all nodes of T_{MAX} with a constant number of operations per node. Since the recursive step only performs operations on T_{MAX} , the complexity of all three algorithms as a function of n and D is only $\mathcal{O}(nD)$, which is *linear* in the length of the time series and the maximum depth. This clearly indicates that the present methods are computationally very efficient and scale well with large numbers of observations. [Taking into account m and p as well, it is easy to see that the complexity is $\mathcal{O}(nD(p^3 + m))$.]

The above discussion also shows that, importantly, all our algorithms can be updated *sequentially*. For example, when observing a new sample x_{n+1} after executing CCTW for x_1^n , only $D + 1$ nodes need to be updated, and $P_e(s, x)$ and $P_{w,s}$ have to be re-computed *only* at these nodes. This takes $\mathcal{O}(D)$ operations, i.e., $\mathcal{O}(1)$ as a function of n . In particular, this implies that sequential prediction can be performed very efficiently. Empirical running times for all forecasting experiments are reported in Appendix E, showing that our methods are much more efficient than essentially all the alternatives examined. The difference is in fact very large, especially when comparing with state-of-the-art ML models that require heavy training and do not allow for efficient sequential updates, giving empirical running times that are typically larger by several orders of magnitude than ours; see also [50] for a relevant review comparing the computational requirements of ML versus statistical techniques.

3.2 Choosing the hyperparameters, quantiser and AR order

It can be seen from Lemma 2 that the posterior distributions of ϕ_s and σ_s^2 are typically not very sensitive to the prior hyperparameters (i.e., when reasonably many observations exist with context s). In all the experimental results below we make the simple choice $\mu_o = 0$ and $\Sigma_o = I$ in the AR coefficients’ prior. In view of equation (10), τ and λ should be chosen to be relatively small in order to minimise their effect on the posterior, while keeping the mode of the inverse-gamma prior, $\lambda/(\tau + 1)$, reasonable. For the context tree prior, we use the default value of $\beta = 1 - 2^{-m+1}$ [42], and the maximum depth $D = 10$.

Finally, we introduce a principled Bayesian way for selecting the quantiser thresholds $\{c_i\}$ of (1) and the AR order p . Viewing them as extra parameters on an additional layer above everything else, we place uniform priors on $\{c_i\}$ and p , and perform Bayesian model selection [60, 48, 61] to obtain their MAP values. The resulting posterior $p(\{c_i\}, p|x)$ is proportional to the *evidence* $p(x|\{c_i\}, p)$, which can be computed exactly using the CCTW algorithm (Theorem 1). So, in order to select appropriate values, we specify a suitable range of possible $\{c_i\}$ and p , and select the ones with the higher evidence. For the AR order we take $1 \leq p \leq p_{\text{max}}$ for an appropriate p_{max} (e.g., $p_{\text{max}} = 5$ in our experiments), and for the $\{c_i\}$ we perform a grid search in a reasonable range (e.g., between the 10th and 90th percentiles of the data). Even though a uniform prior is used for p , we note that the Bayesian approach implicitly penalises more complex models (i.e., larger values of p), by averaging over a larger number of parameters. [This well-known phenomenon [60, 48, 71, 39] is often referred to as “automatic Occam’s Razor”. In fact, the popular BIC model selection criterion [70] can be derived as an asymptotic approximation to the evidence [41].]

3.3 Comparison with other AR mixtures

Threshold AR models. Threshold autoregressive (TAR) models were introduced in [75], and have been used extensively in the analysis of nonlinear time series; see, e.g., the reviews [74, 30] and the texts [17, 76, 73]. Although numerous different versions of TAR models have been employed (see, e.g., the discussion in [74]), the most commonly used one is the self-exciting threshold AR (SETAR) model, which considers partitions of the state space based on the quantised value of x_{n-d} , for some *delay* parameter $d > 0$. Clearly, the BCT-AR model class is much richer and more general.

Mixture AR models. The mixture autoregressive (MAR) models of [83] are a generalisation of the Gaussian mixture transition distribution (GMTD) models of [46]: They consist of a simple linear mixture of K Gaussian AR components. Extensions of MAR models include the conditional heteroscedastic (MAR-ARCH) model [85], the use of exogenous variables [84], and the use of the Student- t distribution to model heavy tails [82], but these models seem less relevant for the type of applications considered here, as their benefits are limited to examples of datasets possessing these specific characteristics (conditional heteroscedasticity, heavy tails, etc.).

When the BCT-AR posterior essentially concentrates on K models, T_1, \dots, T_K , (which was commonly observed in practice), the posterior predictive distribution can be written as,

$$p(x_{n+1}|x) = \sum_{k=1}^K \pi(T_k|x) p(x_{n+1}|T_k, x) ,$$

so that BCT-AR can be viewed as a generalised MAR model, with components corresponding to the AR models at the leaves of each T_k , and with Bayesian weights automatically selected as $\pi(T_k|x)$.

Therefore, the BCT-AR model can be viewed as a *generalisation* of both the MAR and SETAR model classes. Also, it allows for effective Bayesian inference, implicitly overcoming important challenges that arise naturally with SETAR and MAR models, including choosing the delay parameter, the number of components, and the AR orders. The superiority of the proposed approach is verified in the experiments reported in the next section.

4 Experimental results

We evaluate the performance of the BCT-AR model on simulated data and real data from standard applications of nonlinear (univariate) time series from economics and finance, with possibly limited training data. Among all the methods discussed in the Introduction, we compare with the most successful previous approaches for these types of applications, considering both classical and modern ML methods. Useful resources include the R package `forecast` [35] and the Python library ‘GluonTS’ [3, 2], containing implementations of state-of-the-art classical and ML methods, respectively. We briefly discuss the methods used, and refer to the packages’ documentation and Appendix D for more details on the methods themselves and the training procedures carried out.

Among classical statistical approaches, we compare with SETAR and MAR models (using the R packages `TSA` [13] and `mixAR` [9]), and with ARIMA and Exponential smoothing state space (ETS) models (implemented as `auto.arima` [35] and `ets` [33, 36] in `forecast`). Among ML-based techniques, we compare with the Neural Network AR (NNAR) model (implemented in `forecast`), with the most-successful RNN-based approaches, deepAR [69] and N-BEATS [54]

(both implemented in GluonTS), and with the GP time series model from [27], (also implemented in GluonTS). Finally, we note that ‘Prophet’ [72] is another popular classical approach which decomposes the time series to a trend and seasonal component, but it only uses time as a regressor and “treats the forecasting problem as a curve-fitting exercise.” So, it is not well-suited for the applications considered here (which are governed by complex nonlinear dynamics) and, as expected, in practice it was not competitive compared to the presented alternatives.

4.1 Simulated data

We first perform a simulated experiment illustrating that our methods are consistent and effective with data generated by BCT-SSM models. The context tree model used here is the tree of Figure 1, the threshold of the quantiser is $c = 0$, and the AR order is $p = 2$. The exact BCT-AR model is given by:

$$x_n = \begin{cases} 0.7 x_{n-1} - 0.3 x_{n-2} + e_n, & e_n \sim \mathcal{N}(0, 0.15), & \text{if } s = 1: x_{n-1} > 0, \\ -0.3 x_{n-1} - 0.2 x_{n-2} + e_n, & e_n \sim \mathcal{N}(0, 0.10), & \text{if } s = 01: x_{n-1} \leq 0, x_{n-2} > 0, \\ 0.5 x_{n-1} + e_n, & e_n \sim \mathcal{N}(0, 0.05), & \text{if } s = 00: x_{n-1} \leq 0, x_{n-2} \leq 0. \end{cases}$$

We first examine the posterior over trees, $\pi(T|x)$. On a time series consisting of only $n = 100$ observations, the MAP tree identified by the CBCT algorithm is the empty tree corresponding to a single AR model, with posterior probability 99.9%. This means that the data do not provide sufficient evidence to support a more complex state space partition. With $n = 300$ observations, the MAP tree is now the true underlying model, with posterior probability 57%. And with $n = 500$ observations, the posterior of the true model is 99.9%. Therefore, the posterior indeed concentrates on the true model, indicating that the BCT-AR inferential framework can be very effective even with limited training data. The complete BCT-AR model fitted from $n = 1000$ observations with its MAP estimated parameters, shown in (13), clearly indicates that all estimates have essentially converged. In Appendix C.1, we also report values of the evidence $p(x|c, p)$, which is maximised at the true values of $c = 0$ and $p = 2$, verifying that our inferential procedure for choosing them is also effective.

$$x_n = \begin{cases} 0.66 x_{n-1} - 0.19 x_{n-2} + e_n, & e_n \sim \mathcal{N}(0, 0.16), & \text{if } x_{n-1} > 0, \\ -0.39 x_{n-1} - 0.27 x_{n-2} + e_n, & e_n \sim \mathcal{N}(0, 0.12), & \text{if } x_{n-1} \leq 0, x_{n-2} > 0, \\ 0.45 x_{n-1} - 0.03 x_{n-2} + e_n, & e_n \sim \mathcal{N}(0, 0.058), & \text{if } x_{n-1} \leq 0, x_{n-2} \leq 0. \end{cases} \quad (13)$$

Forecasting. We evaluate the performance of our methods in out-of-sample 1-step ahead forecasts, and compare with state-of-the-art approaches in four simulated and three real datasets. The complete descriptions of all datasets can be found in Appendix C. The first simulated dataset (`sim_1`) is generated by the BCT-AR model used above (Appendix C.1), and the second (`sim_2`) by a BCT-AR model with a ternary tree of depth 2 (Appendix C.2). The third and fourth ones (`sim_3` and `sim_4`) are generated from SETAR models of orders $p = 1$ and $p = 5$, respectively (Appendix C.3 and C.4). In each case, the training set consists of the first 50% of the observations; also, we update all models at every time-step in the test set. For BCT-AR, the MAP tree with its MAP parameters is used at every time-step, which can be updated efficiently (Section 3.1). From Table 1, it is observed that our methods outperform the alternatives, and achieve the lowest mean-squared error (MSE) even on the two datasets generated from SETAR models. As discussed in Section 3.2, the BCT-SSM methods also outperform the alternatives in terms of empirical running times, reported in Appendix E.

Table 1: Mean squared error (MSE) of forecasts in simulated and real experiments

	BCT-AR	ARIMA	ETS	NNAR	deepAR	N-BEATS	GP	SETAR	MAR
sim_1	0.131	0.150	0.178	0.143	0.148	0.232	0.181	0.141	0.151
sim_2	0.035	0.050	0.054	0.048	0.061	0.112	0.086	0.050	0.064
sim_3	0.216	0.267	0.293	0.252	0.273	0.357	0.359	0.243	0.283
sim_4	0.891	1.556	1.614	1.287	1.573	2.081	2.046	0.951	1.543
unemp	0.034	0.040	0.042	0.036	0.036	0.054	0.050	0.038	0.037
gnp	0.324	0.364	0.378	0.393	0.473	0.490	0.562	0.394	0.384
ibm	78.02	82.90	77.52	78.90	75.71	77.90	87.27	81.07	77.02

4.2 US unemployment rate

An important application of SETAR models is in modelling the US unemployment rate [30, 52, 76, 67, 43]. As described in [52, 76], the unemployment rate moves countercyclically with business cycles, and rises quickly but decays slowly, indicating nonlinear behaviour. Here, we study the quarterly US unemployment rate in the time period from 1948 to 2019 (dataset `unemp`, 288 observations). Following [52], we consider the difference series $\Delta x_n = x_n - x_{n-1}$, and also include a constant term in the AR model. For the quantiser alphabet size, $m = 2$ is a natural choice here, as will become apparent below. The threshold selected using the procedure of Section 3.2 is $c = 0.15$, and the resulting MAP tree is the tree of Figure 1, with depth $d = 2$, leaves $\{1, 01, 00\}$, and posterior 91.5%. The complete BCT-AR model with its MAP parameters is given below, where $e_n \sim \mathcal{N}(0, 1)$,

$$\Delta x_n = \begin{cases} 0.09 + 0.72 \Delta x_{n-1} - 0.30 \Delta x_{n-2} + 0.42 e_n, & \text{if } \Delta x_{n-1} > 0.15, \\ 0.04 + 0.29 \Delta x_{n-1} - 0.32 \Delta x_{n-2} + 0.32 e_n, & \text{if } \Delta x_{n-1} \leq 0.15, \Delta x_{n-2} > 0.15, \\ -0.02 + 0.34 \Delta x_{n-1} + 0.19 \Delta x_{n-2} + 0.20 e_n, & \text{if } \Delta x_{n-1} \leq 0.15, \Delta x_{n-2} \leq 0.15. \end{cases}$$

Interpretation. The MAP BCT-AR model finds significant structure in the data, providing a very natural interpretation. It identifies 3 meaningful states: First, jumps in the unemployment rate higher than 0.15 signify economic contractions (context 1). If there is not a jump at the most recent time-point, the model looks further back to determine the state. Context 00 signifies a stable economy, as there are no jumps in the unemployment rate for two consecutive quarters. Finally, context 01 identifies an intermediate state: “stabilising just after a contraction”. An important feature identified by the BCT-AR model is that the volatility is different in each case: Higher in contractions ($\sigma = 0.42$), smaller in stable economy regions ($\sigma = 0.20$), and in-between for context 01 ($\sigma = 0.32$).

Forecasting. In addition to its appealing interpretation, the BCT-AR model outperforms all benchmarks in forecasting (Table 1), giving a 6% lower MSE than the second-best methods.

4.3 US Gross National Product

Another important example of nonlinear time series in economics is the US Gross National Product (GNP) [58, 30]. We study the quarterly US GNP in the time period from 1947 to 2019 (dataset `gnp`, 291 observations). Following [58], we consider the difference in the logarithm of the series, $y_n = \log x_n - \log x_{n-1}$.

As above, $m = 2$ is a natural choice for the quantiser size, helping to differentiate economic expansions from contractions – which govern the underlying dynamics. The MAP BCT-AR tree is shown in Figure 2: It has depth $d = 3$, its leaves are $\{0, 10, 110, 111\}$ and its posterior is 42.6%. The complete set of parameters at the leaves are shown in Appendix C.6.

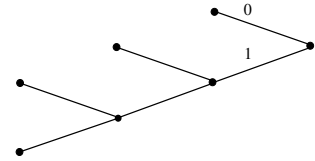


Figure 2: MAP tree model

Interpretation. Compared with the previous example, here the MAP BCT-AR model finds even richer structure in the data and identifies four meaningful states. First, as before, there is a single state corresponding to an economic contraction (which now corresponds to $s = 0$ instead of $s = 1$ as the GNP obviously increases in expansions and decreases in contractions). And again, the model does not look further back whenever a contraction is detected. Here, the model also shows that the effect of a contraction is still present even after *three* quarters ($s = 110$), and that the exact ‘distance’ from a contraction is also important, with the dynamics changing depending on how much time has elapsed. Finally, the state $s = 111$ corresponds to a flourishing, expanding economy, without a contraction in the recent past. An important feature captured by the BCT-AR model is again that the volatility is different in each case. More specifically, it is found that the volatility strictly decreases with the distance from the last contraction, starting with the maximum $\sigma = 1.23$ for $s = 0$, and decreasing to $\sigma = 0.75$ for $s = 111$ (see Appendix C.6).

Forecasting. The BCT-AR model outperforms all benchmarks in forecasting (Table 1), giving a 12% lower MSE than the second-best method; also, it is computationally very efficient (see Appendix E).

4.4 The stock price of IBM

Finally, we examine the daily IBM common stock closing price from May 17, 1961 to November 2, 1962 (dataset `ibm`, 369 observations), taken from [10]. This is a well-studied dataset (e.g. [10, 51, 73, 51, 83]), with [10] fitting an ARIMA model, [73] fitting a SETAR model and [83] fitting a MAR model to the data. Following previous approaches, we consider the first-difference series, $\Delta x_n = x_n - x_{n-1}$. For the alphabet size of the quantiser we choose $m = 3$, with contexts $\{0, 1, 2\}$ naturally corresponding to the states {down, steady, up} for the stock price. Using the procedure of Section 3.2 to select the thresholds, the resulting quantiser regions are: $s = 0$ if $\Delta x_{n-1} < -7$, $s = 2$ if $\Delta x_{n-1} > 7$, and $s = 1$ otherwise. The MAP tree is shown in Figure 3: It has depth $d = 2$, and its leaves are $\{0, 2, 10, 11, 12\}$, hence identifying five states. Its posterior is 99.3%, suggesting that there is very strong evidence in the data supporting this exact structure, even with only 369 observations. The complete BCT-AR model with its MAP parameters is given in Appendix C.7.

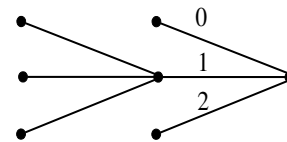


Figure 3: MAP tree model

Interpretation. The BCT-AR model reveals important information about apparent structure in the data, which has not been identified before. Firstly, it admits a very simple and natural interpretation: In order to determine the AR model generating the next value, we need to look back until there is a significant enough price change (corresponding to contexts 0, 2, 10, 12), or until we reach the maximum depth of 2 (context 11). Another important feature captured by this model is the commonly observed asymmetric response in volatility due to positive and negative shocks, sometimes called the *leverage effect* [76, 10]. Even though there is no suggestion

of that in the prior, the MAP model shows that negative shocks increase the volatility much more: Context 0 has the highest volatility ($\sigma = 12.3$), with 10 being a close second ($\sigma = 10.8$), showing that the effect of a past shock is still present. In all other cases the volatility is much smaller (between $\sigma = 5.17$ and $\sigma = 6.86$).

Forecasting. From the results of Table 1, it is observed that in 1-step ahead forecasts deepAR performs marginally better than the alternatives, with BCT-AR, MAR and N-BEATS also having comparable performance. However, as presented in Appendix C.7, the BCT-AR model is found to have the best performance in multi-step ahead forecasts (2-step and 3-step). And because of its efficient sequential updates, it also gives the smallest running times (Appendix E).

5 Limitations and future work

The main requirement potentially limiting the applicability of the proposed methods is that the “estimated probabilities” of (5) need to be evaluated. This leads to several possible directions for future work. First, as discussed in Section 2.3, when the integrals in (5) are not tractable, they could be approximated and used to perform approximate inference for the general BCT-SSM. This way, more general models like ARIMA, ARCH, or even flexible models including GPs and neural networks could be used as building blocks for the BCT-SSM mixture model. Also, more general classes of quantisers can be considered for extracting discrete contexts (see Section 2.1), allowing greater flexibility in the state space partitions and enabling the identification of more complex dependencies in the data. Lastly, extending our methods to multivariate time series is also feasible, and would greatly broaden the scope of applications of our hierarchical Bayesian model.

References

- [1] N.K. Ahmed, A.F. Atiya, N.E. Gayar, and H. El-Shishiny. An empirical comparison of machine learning models for time series forecasting. *Econometric reviews*, 29(5-6):594–621, 2010.
- [2] A. Alexandrov, K. Benidis, M. Bohlke-Schneider, V. Flunkert, J. Gasthaus, T. Januschowski, D.C. Maddix, S. Rangapuram, D. Salinas, J. Schulz, et al. Gluonts: Probabilistic time series models in python. *arXiv preprint arXiv:1906.05264*, 2019.
- [3] A. Alexandrov, K. Benidis, V. Bohlke-Schneider, M. and Flunkert, J. Gasthaus, T. Januschowski, D.C. Maddix, S.S. Rangapuram, D. Salinas, J. Schulz, et al. GluonTS: Probabilistic and neural time series modeling in Python. *Journal of Machine Learning Research*, 21(116):1–6, 2020.
- [4] F.M. Alvarez, A. Troncoso, J.C. Riquelme, and J.S.A. Ruiz. Energy time series forecasting based on pattern sequence similarity. *IEEE Transactions on Knowledge and Data Engineering*, 23(8):1230–1243, 2010.
- [5] S. Alvisi, M. Franchini, and A. Marinelli. A short-term, pattern-based model for water-demand forecasting. *Journal of Hydroinformatics*, 9(1):39–50, 2007.
- [6] C. Andrieu, A. Doucet, and R. Holenstein. Particle Markov chain Monte Carlo methods. *Journal of the Royal Statistical Society: Series B (Statistical Methodology)*, 72(3):269–342, 2010.
- [7] K. Benidis, S.S. Rangapuram, V. Flunkert, B. Wang, D. Maddix, C. Turkmen, J. Gasthaus, M. Bohlke-Schneider, D. Salinas, L. Stella, et al. Neural forecasting: Introduction and literature overview. *arXiv preprint arXiv:2004.10240*, 2020.

- [8] D.J. Berndt and J. Clifford. Using dynamic time warping to find patterns in time series. In *KDD Workshop*, volume 10, pages 359–370. Seattle, WA, USA, 1994.
- [9] G. N. Boshnakov and D. Ravagli. *mixAR: Mixture Autoregressive Models*, 2021. R package version 0.22.5. <https://CRAN.R-project.org/package=mixAR>.
- [10] G.E.P. Box, G.M. Jenkins, G.C. Reinsel, and G.M. Ljung. *Time series analysis: forecasting and control*. John Wiley & Sons, 2015.
- [11] J.Q. Candela, A. Girard, J. Larsen, and C.E. Rasmussen. Propagation of uncertainty in bayesian kernel models-application to multiple-step ahead forecasting. In *2003 IEEE International Conference on Acoustics, Speech, and Signal Processing, 2003. Proceedings.(ICASSP'03).*, volume 2, pages II–701. IEEE, 2003.
- [12] K.S. Chan. Consistency and limiting distribution of the least squares estimator of a threshold autoregressive model. *Annals of Statistics*, 21(1):520–533, 1993.
- [13] K.S. Chan and B. Ripley. *TSA: Time Series Analysis*, 2020. R package version 1.3. <https://CRAN.R-project.org/package=TSA>.
- [14] S. Chib. Marginal likelihood from the Gibbs output. *Journal of the american statistical association*, 90(432):1313–1321, 1995.
- [15] S. Chib and I. Jeliazkov. Marginal likelihood from the Metropolis–Hastings output. *Journal of the American statistical association*, 96(453):270–281, 2001.
- [16] J. Chung, K. Kastner, L. Dinh, K. Goel, A.C. Courville, and Y. Bengio. A recurrent latent variable model for sequential data. *Advances in neural information processing systems*, 28, 2015.
- [17] J.D. Cryer and K.S. Chan. *Time series analysis: with applications in R*. Springer Science & Business Media, 2008.
- [18] A. Doucet, N. De Freitas, N.J. Gordon, et al. *Sequential Monte Carlo methods in practice*. Springer, 2001.
- [19] J. Durbin and S.J. Koopman. *Time series analysis by state space methods*, volume 38. OUP Oxford, 2012.
- [20] S. Eleftheriadis, T. Nicholson, M. Deisenroth, and J. Hensman. Identification of Gaussian process state space models. *Advances in neural information processing systems*, 30, 2017.
- [21] C. Faloutsos, J. Gasthaus, T. Januschowski, and Y. Wang. Forecasting big time series: old and new. *Proceedings of the VLDB Endowment*, 11(12):2102–2105, 2018.
- [22] N. Friel and A.N. Pettitt. Marginal likelihood estimation via power posteriors. *Journal of the Royal Statistical Society: Series B (Statistical Methodology)*, 70(3):589–607, 2008.
- [23] R. Frigola. *Bayesian time series learning with Gaussian processes*. PhD thesis, University of Cambridge, 2015.
- [24] R. Frigola, Y. Chen, and C.E. Rasmussen. Variational Gaussian process state-space models. *Advances in neural information processing systems*, 27, 2014.
- [25] R. Frigola, F. Lindsten, T.B. Schön, and C.Ed. Rasmussen. Bayesian inference and learning in Gaussian process state-space models with particle MCMC. *Advances in neural information processing systems*, 26, 2013.
- [26] T.C. Fu, F.L. Chung, R. Luk, and C.M. Ng. Stock time series pattern matching: Template-based vs. rule-based approaches. *Engineering Applications of Artificial Intelligence*, 20(3):347–364, 2007.
- [27] A. Girard, C. Rasmussen, J.Q. Candela, and R. Murray-Smith. Gaussian process priors with uncertain inputs application to multiple-step ahead time series forecasting. *Advances in neural information processing systems*, 15, 2002.

- [28] A. Graves. Generating sequences with recurrent neural networks. *arXiv preprint arXiv:1308.0850*, 2013.
- [29] J.D. Hamilton. *Time series analysis*. Princeton university press, 2020.
- [30] B.E. Hansen. Threshold autoregression in economics. *Statistics and its Interface*, 4(2):123–127, 2011.
- [31] S. Hochreiter and J. Schmidhuber. Long short-term memory. *Neural computation*, 9(8):1735–1780, 1997.
- [32] Q. Hu, P. Su, D. Yu, and J. Liu. Pattern-based wind speed prediction based on generalized principal component analysis. *IEEE Transactions on Sustainable Energy*, 5(3):866–874, 2014.
- [33] R. Hyndman, A.B. Koehler, J.K. Ord, and R.D. Snyder. *Forecasting with exponential smoothing: the state space approach*. Springer Science & Business Media, 2008.
- [34] R. J. Hyndman. *fma: Data sets from "Forecasting: methods and applications" by Makridakis, Wheelwright & Hyndman (1998)*, 2020. R package version 2.4. <https://cran.r-project.org/package=fma>.
- [35] R.J. Hyndman and Y. Khandakar. Automatic time series forecasting: the forecast package for R. *Journal of Statistical Software*, 26(3):1–22, 2008. <https://CRAN.R-project.org/package=forecast>.
- [36] R.J. Hyndman, A.B. Koehler, R.D. Snyder, and S. Grose. A state space framework for automatic forecasting using exponential smoothing methods. *International Journal of forecasting*, 18(3):439–454, 2002.
- [37] R.E. Kalman. A new approach to linear filtering and prediction problems. *Transactions of the American Society of Mathematical Engineering, Journal of Basic Engineering*, 82(D):35–45, 1960.
- [38] M. Karl, M. Soelch, J. Bayer, and P. Van der Smagt. Deep variational bayes filters: Unsupervised learning of state space models from raw data. *arXiv preprint arXiv:1605.06432*, 2016.
- [39] R.E. Kass and A.E. Raftery. Bayes factors. *Journal of the American Statistical Association*, 90(430):773–795, 1995.
- [40] D.P. Kingma and M. Welling. Auto-encoding variational bayes. *arXiv preprint arXiv:1312.6114*, 2013.
- [41] S. Konishi and G. Kitagawa. *Information criteria and statistical modeling*. Springer Science & Business Media, 2008.
- [42] I. Kontoyiannis, L. Mertzanis, A. Panotopoulou, I. Papageorgiou, and M. Skoularidou. Bayesian Context Trees: Modelling and exact inference for discrete time series. *Journal of the Royal Statistical Society: Series B (Statistical Methodology)*, April 2022. <https://doi.org/10.1111/rssb.12511>.
- [43] G. Koop and S.M. Potter. Dynamic asymmetries in US unemployment. *Journal of Business & Economic Statistics*, 17(3):298–312, 1999.
- [44] R. Krishnan, U. Shalit, and D. Sontag. Structured inference networks for nonlinear state space models. In *Proceedings of the AAAI Conference on Artificial Intelligence*, 2017.
- [45] R.G. Krishnan, U. Shalit, and D. Sontag. Deep kalman filters. *arXiv preprint arXiv:1511.05121*, 2015.
- [46] N.D. Le, R.D. Martin, and A.E. Raftery. Modeling flat stretches, bursts outliers in time series using mixture transition distribution models. *Journal of the American Statistical Association*, 91(436):1504–1515, 1996.
- [47] X. Liu, Z. Ni, D. Yuan, Y. Jiang, Z. Wu, J. Chen, and Y. Yang. A novel statistical time-series pattern based interval forecasting strategy for activity durations in workflow systems. *Journal of Systems and Software*, 84(3):354–376, 2011.

- [48] D.J.C. MacKay. Bayesian interpolation. *Neural Computation*, 4(3):415–447, 1992.
- [49] S. Makridakis, E. Spiliotis, and V. Assimakopoulos. The M4 Competition: Results, findings, conclusion and way forward. *International Journal of Forecasting*, 34(4):802–808, 2018.
- [50] S. Makridakis, E. Spiliotis, and V. Assimakopoulos. Statistical and machine learning forecasting methods: Concerns and ways forward. *PloS one*, 13(3):e0194889, 2018.
- [51] S. Makridakis, S. Wheelwright, and R.J. Hyndman. *Forecasting: methods and applications*. John Wiley & Sons, 1998.
- [52] A.L. Montgomery, V. Zarnowitz, R.S. Tsay, and G.C. Tiao. Forecasting the US unemployment rate. *Journal of the American Statistical Association*, 93(442):478–493, 1998.
- [53] R. Murray-Smith and A. Girard. Gaussian Process priors with ARMA noise models. In *Irish Signals and Systems Conference, Maynooth*, volume 147, page 152. Citeseer, 2001.
- [54] B.N. Oreshkin, D. Carпов, N. Chapados, and Y. Bengio. N-BEATS: Neural basis expansion analysis for interpretable time series forecasting. *arXiv preprint arXiv:1905.10437*, 2019.
- [55] G. Ouyang, C. Dang, D.A. Richards, and X. Li. Ordinal pattern based similarity analysis for eeg recordings. *Clinical Neurophysiology*, 121(5):694–703, 2010.
- [56] I. Papageorgiou and I. Kontoyiannis. Posterior representations for Bayesian Context Trees: Sampling, estimation and convergence. *arXiv preprint arXiv:2202.02239*, 2022.
- [57] I. Papageorgiou, I. Kontoyiannis, L. Mertzanis, A. Panotopoulou, and M. Skoularidou. Revisiting context-tree weighting for Bayesian inference. In *2021 IEEE International Symposium on Information Theory (ISIT)*, pages 2906–2911, 2021.
- [58] S.M. Potter. A nonlinear approach to US GNP. *Journal of applied econometrics*, 10(2):109–125, 1995.
- [59] S.S. Rangapuram, M.W. Seeger, J. Gasthaus, L. Stella, Y. Wang, and T. Januschowski. Deep state space models for time series forecasting. *Advances in neural information processing systems*, 31, 2018.
- [60] C.E. Rasmussen and Z. Ghahramani. Occam’s razor. *Advances in Neural Information Processing Systems*, pages 294–300, 2001.
- [61] C.E. Rasmussen and C.K.I. Williams. *Gaussian processes for machine learning*. MIT Press, 2006.
- [62] D.J. Rezende, S. Mohamed, and D. Wierstra. Stochastic backpropagation and approximate inference in deep generative models. In *International conference on machine learning*, pages 1278–1286. PMLR, 2014.
- [63] J. Rissanen. A universal data compression system. *IEEE Transactions on Information Theory*, 29(5):656–664, 1983.
- [64] J. Rissanen. A universal prior for integers and estimation by minimum description length. *Annals of Statistics*, 11(2):416–431, 1983.
- [65] J. Rissanen. Complexity of strings in the class of markov sources. *IEEE Transactions on Information Theory*, 32(4):526–532, 1986.
- [66] S. Roberts, M. Osborne, M. Ebden, S. Reece, N. Gibson, and S. Aigrain. Gaussian processes for time-series modelling. *Philosophical Transactions of the Royal Society A: Mathematical, Physical and Engineering Sciences*, 371(1984):20110550, 2013.
- [67] P. Rothman. Forecasting asymmetric unemployment rates. *Review of Economics and Statistics*, 80(1):164–168, 1998.

- [68] E. Sabeti, P.X.K. Song, and A.O. Hero. Pattern-based analysis of time series: Estimation. In *2020 IEEE International Symposium on Information Theory (ISIT)*, pages 1236–1241, 2020.
- [69] D. Salinas, V. Flunkert, J. Gasthaus, and T. Januschowski. DeepAR: Probabilistic forecasting with autoregressive recurrent networks. *International Journal of Forecasting*, 36(3):1181–1191, 2020.
- [70] G. Schwarz. Estimating the dimension of a model. *Annals of Statistics*, 6(2):461–464, 1978.
- [71] A.F.M. Smith and D.J. Spiegelhalter. Bayes factors and choice criteria for linear models. *Journal of the Royal Statistical Society: Series B (Methodological)*, 42(2):213–220, 1980.
- [72] S.J. Taylor and B. Letham. Forecasting at scale. *The American Statistician*, 72(1):37–45, 2018.
- [73] H. Tong. *Non-linear time series: a dynamical system approach*. Oxford University Press, 1990.
- [74] H. Tong. Threshold models in time series analysis—30 years on. *Statistics and its Interface*, 4(2):107–118, 2011.
- [75] H. Tong and K.S. Lim. Threshold autoregression, limit cycles and cyclical data. *Journal of the Royal Statistical Society: Series B (Statistical Methodology)*, 42(3):245–268, 1980.
- [76] R.S. Tsay. *Analysis of financial time series*, volume 543. John Wiley & Sons, 2005.
- [77] R. Turner, M. Deisenroth, and C.E. Rasmussen. State-space inference and learning with Gaussian processes. In *Proceedings of the Thirteenth International Conference on Artificial Intelligence and Statistics*, pages 868–875. JMLR Workshop and Conference Proceedings, 2010.
- [78] R. D. Turner. *Gaussian processes for state space models and change point detection*. PhD thesis, University of Cambridge, 2012.
- [79] M.J. Weinberger, N. Merhav, and M. Feder. Optimal sequential probability assignment for individual sequences. *IEEE Transactions on Information Theory*, 40(2):384–396, 1994.
- [80] F.M.J. Willems. The context-tree weighting method: extensions. *IEEE Transactions on Information Theory*, 44(2):792–798, 1998.
- [81] F.M.J. Willems, Y.M. Shtarkov, and T.J. Tjalkens. The context-tree weighting method: basic properties. *IEEE Transactions on Information Theory*, 41(3):653–664, 1995.
- [82] C. S. Wong, W. S. Chan, and P. L. Kam. A student t-mixture autoregressive model with applications to heavy-tailed financial data. *Biometrika*, 96(3):751–760, 2009.
- [83] C. S. Wong and W. K. Li. On a mixture autoregressive model. *Journal of the Royal Statistical Society: Series B (Statistical Methodology)*, 62(1):95–115, 2000.
- [84] C. S. Wong and W. K. Li. On a logistic mixture autoregressive model. *Biometrika*, 88(3):833–846, 2001.
- [85] C. S. Wong and W. K. Li. On a mixture autoregressive conditional heteroscedastic model. *Journal of the American Statistical Association*, 96(455):982–995, 2001.
- [86] S.N. Wood. Fast stable restricted maximum likelihood and marginal likelihood estimation of semi-parametric generalized linear models. *Journal of the Royal Statistical Society: Series B (Statistical Methodology)*, 73(1):3–36, 2011.
- [87] H.F. Yu, N. Rao, and I.S. Dhillon. Temporal regularized matrix factorization for high-dimensional time series prediction. *Advances in neural information processing systems*, 29, 2016.
- [88] G. Zhang, B.E. Patuwo, and M.Y. Hu. Forecasting with artificial neural networks: The state of the art. *International journal of forecasting*, 14(1):35–62, 1998.
- [89] X. Zheng, M. Zaheer, A. Ahmed, Y. Wang, E.P. Xing, and A.J. Smola. State space LSTM models with particle MCMC inference. *arXiv preprint arXiv:1711.11179*, 2017.

Appendix

A Proofs of Theorems 1 and 2

The important observation here is that using our different form of the estimated probabilities $P_e(s, x)$ in (5), it is still possible to factorise the marginal likelihoods $p(x|T)$ for the general BCT-SSM as,

$$p(x|T) = \int p(x|\theta, T)\pi(\theta|T)d\theta = \int \prod_{s \in T} \left(\prod_{i \in B_s} p(x_i|T, \theta_s, x_{-D+1}^{i-1}) \pi(\theta_s) d\theta_s \right) = \prod_{s \in T} P_e(s, x),$$

where the second equality follows from the likelihood of the general BCT-SSM in (2), and the fact that we use independent priors on the parameters at the leaves, so that $\pi(\theta|T) = \prod_{s \in T} \pi(\theta_s)$.

Then, the proofs of Theorems 1 and 2 follow along the same lines as the proofs of the corresponding results for discrete time series in [42], with the main difference being that our new general version of the estimated probabilities $P_e(s, x)$ of (5) need to be used in place of their simple discrete versions. Before giving the proofs of the theorems, we recall a useful property for the BCT prior $\pi_D(T)$. Let $\Lambda = \{\lambda\}$ denote the empty tree consisting only of the root node λ . Any tree $T \neq \Lambda$ can be expressed as the union $T = \cup_j T_j$ of a collection of m subtrees T_0, T_1, \dots, T_{m-1} , and its prior can be decomposed as [42]:

Lemma A. *If $T \in \mathcal{T}(D)$, $T \neq \Lambda$, is expressed as the union $T = \cup_j T_j$ of the subtrees $T_j \in \mathcal{T}(D-1)$, then,*

$$\pi_D(T) = \alpha^{m-1} \prod_{j=0}^{m-1} \pi_{D-1}(T_j). \quad (14)$$

A.1 Proof of Theorem 1

The proof is by induction. We want to show that:

$$P_{w,\lambda} = p(x) = \sum_{T \in \mathcal{T}(D)} \pi(T)p(x|T) = \sum_{T \in \mathcal{T}(D)} \pi_D(T) \prod_{s \in T} P_e(s, x). \quad (15)$$

We claim that the following more general statement holds: For any node s at depth d with $0 \leq d \leq D$, we have,

$$P_{w,s} = \sum_{U \in \mathcal{T}(D-d)} \pi_{D-d}(U) \prod_{u \in U} P_e(su, x), \quad (16)$$

where su denotes the concatenation of contexts s and u .

Clearly (16) implies (15) upon taking $s = \lambda$ (i.e., with $d = 0$). Also, (16) is trivially true for nodes s at level D , since it reduces to the fact that $P_{w,s} = P_{e,s}$ for leaves s , by definition.

Suppose (16) holds for all nodes s at depth d for some fixed $0 < d \leq D$. Let s be a node at depth $d-1$; then, by the inductive hypothesis,

$$\begin{aligned} P_{w,s} &= \beta P_e(s, x) + (1 - \beta) \prod_{j=0}^{m-1} P_{w,sj} \\ &= \beta P_e(s, x) + (1 - \beta) \prod_{j=0}^{m-1} \left[\sum_{T_j \in \mathcal{T}(D-d)} \pi_{D-d}(T_j) \prod_{t \in T_j} P_e(sj t, x) \right], \end{aligned}$$

where sjt denotes the concatenation of context s , then symbol j , then context t , in that order.

So,

$$\begin{aligned} P_{w,s} &= \beta P_e(s, x) + (1 - \beta) \sum_{T_0, T_1, \dots, T_{m-1} \in \mathcal{T}(D-d)} \prod_{j=0}^{m-1} \left[\pi_{D-d}(T_j) \prod_{t \in T_j} P_e(sjt, x) \right] \\ &= \beta P_e(s, x) + \frac{1 - \beta}{\alpha^{m-1}} \sum_{T_0, T_1, \dots, T_{m-1} \in \mathcal{T}(D-d)} \pi_{D-d+1}(\cup_j T_j) \left[\prod_{j=0}^{m-1} \prod_{t \in T_j} P_e(sjt, x) \right], \end{aligned}$$

where for the last step we have used (14) from Lemma A.

Concatenating every symbol j with every leaf of the corresponding tree T_j , we end up with all the leaves of the larger tree $\cup_j T_j$. Therefore,

$$P_{w,s} = \beta P_e(s, x) + \frac{1 - \beta}{\alpha^{m-1}} \sum_{T_0, T_1, \dots, T_{m-1} \in \mathcal{T}(D-d)} \pi_{D-d+1}(\cup_j T_j) \prod_{t \in \cup_j T_j} P_e(st, x),$$

and since $1 - \beta = \alpha^{m-1}$ and $\pi_d(\Lambda) = \beta$ for all $d \geq 1$,

$$\begin{aligned} P_{w,s} &= \pi_{D-d+1}(\Lambda) P_e(s, x) + \sum_{T_0, T_1, \dots, T_{m-1} \in \mathcal{T}(D-d)} \pi_{D-d+1}(\cup_j T_j) \prod_{t \in \cup_j T_j} P_e(st, x) \\ &= \pi_{D-d+1}(\Lambda) P_e(s, x) + \sum_{T \in \mathcal{T}(D-d+1), T \neq \Lambda} \pi_{D-d+1}(T) \prod_{t \in T} P_e(st, x) \\ &= \sum_{T \in \mathcal{T}(D-d+1)} \pi_{D-d+1}(T) \prod_{t \in T} P_e(st, x). \end{aligned}$$

This establishes (16) for all nodes s at depth $d - 1$, completing the inductive step and the proof of the theorem. \square

A.2 Proof of Theorem 2

As the proof follows very much along the same lines as that of Theorem 3.2 of [42], most of the details are omitted here.

The proof is again by induction. First, we claim that:

$$P_{m,\lambda} = \max_{T \in \mathcal{T}(D)} p(x, T) = \max_{T \in \mathcal{T}(D)} \pi_D(T) \prod_{s \in T} P_e(s, x). \quad (17)$$

As in the proof of Theorem 1, in fact we claim that the following more general statement holds: For any node s at depth d with $0 \leq d \leq D$, we have,

$$P_{m,s} = \max_{U \in \mathcal{T}(D-d)} \pi_{D-d}(U) \prod_{u \in U} P_e(su, x), \quad (18)$$

where su denotes the concatenation of contexts s and u . The proof of this is by an inductive step similar to that of Theorem 1. Taking $s = \lambda$ in (18) implies (17).

Then, it is sufficient to show that for the tree T_1^* that is produced by the CBCT algorithm, $P_{m,\lambda} = p(x, T_1^*)$. This is again proved by induction, via an argument similar to the ones in the previous two cases.

Finally, using (17) and dividing both sides with $p(x)$ completes the proof, since we get:

$$\max_{T \in \mathcal{T}(D)} \pi(T|x) = \pi(T_1^*|x).$$

\square

A.3 The k -CBCT algorithm

The k -BCT algorithm of [42] can be generalised in a similar manner to the way the CTW and BCT algorithms were generalised. The resulting algorithm identifies the top- k *a posteriori* most likely context trees. The proof of the theorem claiming this is similar to the proof of Theorem 3.3 of [42] and thus omitted. Again, the important difference, both in the algorithm description and in the proof, is that the estimated probabilities $P_e(s, x)$ are used in place of their simple discrete version $P_e(a_s)$.

B Proofs of Lemmas 1 and 2

The proofs of these lemmas are mostly based on explicit computations. Recall that, for each context s , the set B_s consists of those indices $i \in \{1, 2, \dots, n\}$ such that the context of x_i is s . The important step in the following two proofs is the factorisation of the likelihood using the sets B_s . In order to prove the lemmas for the AR model with parameters $\theta_s = (\phi_s, \sigma_s^2)$, we first consider an intermediate step in which we assume the noise variance to be known and equal to σ^2 .

B.1 Known noise variance

Here, to any leaf s of the context tree T , we associate an AR model with known variance σ^2 , so that,

$$x_n = \phi_{s,1}x_{n-1} + \dots + \phi_{s,p}x_{n-p} + e_n = \phi_s^\top \tilde{\mathbf{x}}_{n-1} + e_n, \quad e_n \sim \mathcal{N}(0, \sigma^2). \quad (19)$$

In this setting, the parameters of the model are only the AR coefficients $\theta_s = \phi_s$. For these, we use a Gaussian prior,

$$\theta_s \sim \mathcal{N}(\mu_o, \Sigma_o), \quad (20)$$

where μ_o, Σ_o are hyperparameters. In this setting we prove the following for the estimated probabilities $P_e(s, x)$.

Lemma B. *The estimated probabilities $P_e(s, x)$ for the known-variance case are given by,*

$$P_e(s, x) = \frac{1}{(2\pi\sigma^2)^{|B_s|/2}} \frac{1}{\sqrt{\det(I + \Sigma_o S_3 / \sigma^2)}} \exp \left\{ -\frac{E_s}{2\sigma^2} \right\}, \quad (21)$$

where I is the identity matrix and E_s is given by:

$$E_s = \mathbf{s}_1 + \sigma^2 \mu_o^\top \Sigma_o^{-1} \mu_o - (\mathbf{s}_2 + \sigma^2 \Sigma_o^{-1} \mu_o)^\top (S_3 + \sigma^2 \Sigma_o^{-1})^{-1} (\mathbf{s}_2 + \sigma^2 \Sigma_o^{-1} \mu_o). \quad (22)$$

Proof. For the AR model of (19),

$$p(x_i | T, \theta_s, x_{-D+1}^{i-1}) = \frac{1}{\sqrt{2\pi\sigma^2}} \exp \left\{ -\frac{1}{2\sigma^2} (x_i - \theta_s^\top \tilde{\mathbf{x}}_{i-1})^2 \right\},$$

so that,

$$\prod_{i \in B_s} p(x_i | T, \theta_s, x_{-D+1}^{i-1}) = \frac{1}{(\sqrt{2\pi\sigma^2})^{|B_s|}} \exp \left\{ -\frac{1}{2\sigma^2} \sum_{i \in B_s} (x_i - \theta_s^\top \tilde{\mathbf{x}}_{i-1})^2 \right\}.$$

Expanding the sum in the exponent gives,

$$\begin{aligned} \sum_{i \in B_s} (x_i - \theta_s^\top \tilde{\mathbf{x}}_{i-1})^2 &= \sum_{i \in B_s} x_i^2 - 2\theta_s^\top \sum_{i \in B_s} x_i \tilde{\mathbf{x}}_{i-1} + \theta_s^\top \sum_{i \in B_s} \tilde{\mathbf{x}}_{i-1} \tilde{\mathbf{x}}_{i-1}^\top \theta_s \\ &= s_1 - 2\theta_s^\top \mathbf{s}_2 + \theta_s^\top S_3 \theta_s, \end{aligned}$$

from which we obtain that,

$$\begin{aligned} \prod_{i \in B_s} p(x_i | T, \theta_s, x_{-D+1}^{i-1}) &= \frac{1}{(\sqrt{2\pi\sigma^2})^{|B_s|}} \exp \left\{ -\frac{1}{2\sigma^2} (s_1 - 2\theta_s^\top \mathbf{s}_2 + \theta_s^\top S_3 \theta_s) \right\} \\ &= (\sqrt{2\pi})^p \rho_s \mathcal{N}(\theta_s; \boldsymbol{\mu}, S), \end{aligned}$$

by completing the square, where $\boldsymbol{\mu} = S_3^{-1} \mathbf{s}_2$, $S = \sigma^2 S_3^{-1}$, and,

$$\rho_s = \sqrt{\frac{\det(\sigma^2 S_3^{-1})}{(2\pi\sigma^2)^{|B_s|}}} \exp \left\{ -\frac{1}{2\sigma^2} (s_1 - \mathbf{s}_2^\top S_3^{-1} \mathbf{s}_2) \right\}. \quad (23)$$

So, multiplying with the prior:

$$\prod_{i \in B_s} p(x_i | T, \theta_s, x_{-D+1}^{i-1}) \pi(\theta_s) = (\sqrt{2\pi})^p \rho_s \mathcal{N}(\theta_s; \boldsymbol{\mu}, S) \mathcal{N}(\theta_s; \mu_o, \Sigma_o) = \rho_s Z_s \mathcal{N}(\theta_s; \mathbf{m}, \Sigma),$$

where $\Sigma^{-1} = \Sigma_o^{-1} + S^{-1}$, $\mathbf{m} = \Sigma (\Sigma_o^{-1} \mu_o + S^{-1} \boldsymbol{\mu})$, and,

$$Z_s = \frac{1}{\sqrt{\det(\Sigma_o + \sigma^2 S_3^{-1})}} \exp \left\{ -\frac{1}{2} (\mu_o - S_3^{-1} \mathbf{s}_2)^\top (\Sigma_o + \sigma^2 S_3^{-1})^{-1} (\mu_o - S_3^{-1} \mathbf{s}_2) \right\}. \quad (24)$$

Therefore,

$$\prod_{i \in B_s} p(x_i | T, \theta_s, x_{-D+1}^{i-1}) \pi(\theta_s) = \rho_s Z_s \mathcal{N}(\theta_s; \mathbf{m}, \Sigma), \quad (25)$$

and hence,

$$P_e(s, x) = \int \prod_{i \in B_s} p(x_i | T, \theta_s, x_{-D+1}^{i-1}) \pi(\theta_s) d\theta_s = \rho_s Z_s.$$

Using standard matrix inversion properties, after some algebra the product $\rho_s Z_s$ can be rearranged to give exactly the required expression in (21). \square

B.2 Proof of Lemma 1

Now, we move back to the original case, as described in the paper, where the noise variance is considered to be a parameter of the AR model, so that $\theta_s = (\boldsymbol{\phi}_s, \sigma_s^2)$. Here, the joint prior on the parameters is $\pi(\theta_s) = \pi(\boldsymbol{\phi}_s | \sigma_s^2) \pi(\sigma_s^2)$, where,

$$\sigma_s^2 \sim \text{Inv-Gamma}(\tau, \lambda), \quad (26)$$

$$\boldsymbol{\phi}_s | \sigma_s^2 \sim \mathcal{N}(\mu_o, \sigma_s^2 \Sigma_o), \quad (27)$$

and where $(\tau, \lambda, \mu_o, \Sigma_o)$ are hyperparameters.

For $P_e(s, x)$, we just need to compute the integral:

$$P_e(s, x) = \int \prod_{i \in B_s} p(x_i | T, \theta_s, x_{-D+1}^{i-1}) \pi(\theta_s) d\theta_s \quad (28)$$

$$= \int \pi(\sigma_s^2) \left(\int \prod_{i \in B_s} p(x_i | T, \phi_s, \sigma_s^2, x_{-D+1}^{i-1}) \pi(\phi_s | \sigma_s^2) d\phi_s \right) d\sigma_s^2. \quad (29)$$

The inner integral has exactly the form of the estimated probabilities $P_e(s, x)$ from the previous section, where the noise variance was fixed. The only difference is that the prior $\pi(\phi_s | \sigma_s^2)$ of (27) now has covariance matrix $\sigma_s^2 \Sigma_o$ instead of Σ_o . So, using (21)-(22), with Σ_o replaced by $\sigma_s^2 \Sigma_o$, we get,

$$P_e(s, x) = \int \pi(\sigma_s^2) \left\{ C_s^{-1} \left(\frac{1}{\sigma_s^2} \right)^{|B_s|/2} \exp \left(- \frac{D_s}{2\sigma_s^2} \right) \right\} d\sigma_s^2,$$

with C_s and D_s as in Lemma 1. And using the inverse-gamma prior $\pi(\sigma_s^2)$ of (26),

$$P_e(s, x) = C_s^{-1} \frac{\lambda^\tau}{\Gamma(\tau)} \int \left(\frac{1}{\sigma_s^2} \right)^{\tau'+1} \exp \left(- \frac{\lambda'}{\sigma_s^2} \right) d\sigma_s^2, \quad (30)$$

with $\tau' = \tau + \frac{|B_s|}{2}$ and $\lambda' = \lambda + \frac{D_s}{2}$.

The integral in (30) has the form of an inverse-gamma density with parameters τ' and λ' . Its closed-form solution, as required, completes the proof of the lemma:

$$P_e(s, x) = C_s^{-1} \frac{\lambda^\tau}{\Gamma(\tau)} \frac{\Gamma(\tau')}{(\lambda')^{\tau'}}.$$

□

B.3 Proof of Lemma 2

In order to derive the required expressions for the posterior distributions of ϕ_s and σ_s^2 , for a leaf s of model T , first consider the joint posterior $\pi(\theta_s | T, x) = \pi(\phi_s, \sigma_s^2 | T, x)$, given by,

$$\pi(\theta_s | T, x) \propto p(x | T, \theta_s) \pi(\theta_s) = \prod_{i=1}^n p(x_i | T, \theta_s, x_{-D+1}^{i-1}) \pi(\theta_s) \propto \prod_{i \in B_s} p(x_i | T, \theta_s, x_{-D+1}^{i-1}) \pi(\theta_s),$$

where we used the fact that, in the product, only the terms involving indices $i \in B_s$ are functions of θ_s . So,

$$\pi(\phi_s, \sigma_s^2 | T, x) \propto \left(\prod_{i \in B_s} p(x_i | T, \phi_s, \sigma_s^2, x_{-D+1}^{i-1}) \pi(\phi_s | \sigma_s^2) \right) \pi(\sigma_s^2).$$

Here, the first two terms can be computed from (25) of the previous section, where the noise variance was known. Again, the only difference is that we have to replace Σ_o with $\sigma_s^2 \Sigma_o$ because of the prior $\pi(\phi_s | \sigma_s^2)$ defined in (27). After some algebra, this gives,

$$\pi(\phi_s, \sigma_s^2 | T, x) \propto \left(\frac{1}{\sigma_s^2} \right)^{|B_s|/2} \exp \left(- \frac{D_s}{2\sigma_s^2} \right) \mathcal{N}(\phi_s; \mathbf{m}_s, \Sigma_s) \pi(\sigma_s^2),$$

with \mathbf{m}_s defined as in Lemma 2, and $\Sigma_s = \sigma_s^2 (S_3 + \Sigma_o^{-1})^{-1}$.

Substituting the prior $\pi(\sigma_s^2)$ in the last expression,

$$\pi(\boldsymbol{\phi}_s, \sigma_s^2 | T, x) \propto \left(\frac{1}{\sigma_s^2} \right)^{\tau+1+|B_s|/2} \exp \left(- \frac{\lambda + D_s/2}{\sigma_s^2} \right) \mathcal{N}(\boldsymbol{\phi}_s; \mathbf{m}_s, \Sigma_s). \quad (31)$$

From (31), it is easy to integrate out $\boldsymbol{\phi}_s$ and get the posterior of σ_s^2 ,

$$\pi(\sigma_s^2 | T, x) = \int \pi(\boldsymbol{\phi}_s, \sigma_s^2 | T, x) d\boldsymbol{\phi}_s \propto \left(\frac{1}{\sigma_s^2} \right)^{\tau+1+|B_s|/2} \exp \left(- \frac{\lambda + D_s/2}{\sigma_s^2} \right),$$

which is of the form of an inverse-gamma distribution with parameters $\tau' = \tau + \frac{|B_s|}{2}$ and $\lambda' = \lambda + \frac{D_s}{2}$, proving the first part of the lemma.

However, as Σ_s is a function of σ_s^2 , integrating out σ_s^2 requires more algebra. We have,

$$\begin{aligned} \mathcal{N}(\boldsymbol{\phi}_s; \mathbf{m}_s, \Sigma_s) &\propto \frac{1}{\sqrt{\det(\Sigma_s)}} \exp \left\{ - \frac{1}{2} (\boldsymbol{\phi}_s - \mathbf{m}_s)^T \Sigma_s^{-1} (\boldsymbol{\phi}_s - \mathbf{m}_s) \right\} \\ &\propto \left(\frac{1}{\sigma_s^2} \right)^{p/2} \exp \left\{ - \frac{1}{2\sigma_s^2} (\boldsymbol{\phi}_s - \mathbf{m}_s)^T (S_3 + \Sigma_o^{-1}) (\boldsymbol{\phi}_s - \mathbf{m}_s) \right\}, \end{aligned}$$

and substituting this in (31) gives that $\pi(\boldsymbol{\phi}_s, \sigma_s^2 | T, x)$ is proportional to,

$$\left(\frac{1}{\sigma_s^2} \right)^{\tau+1+\frac{|B_s|+p}{2}} \exp \left\{ - \frac{1}{2\sigma_s^2} \left(2\lambda + D_s + (\boldsymbol{\phi}_s - \mathbf{m}_s)^T (S_3 + \Sigma_o^{-1}) (\boldsymbol{\phi}_s - \mathbf{m}_s) \right) \right\},$$

which as a function of σ_s^2 has the form of an inverse-gamma density, allowing us to integrate out σ_s^2 . Denoting $L = 2\lambda + D_s + (\boldsymbol{\phi}_s - \mathbf{m}_s)^T (S_3 + \Sigma_o^{-1}) (\boldsymbol{\phi}_s - \mathbf{m}_s)$, and $\tilde{\tau} = \tau + \frac{|B_s|+p}{2}$,

$$\pi(\boldsymbol{\phi}_s | T, x) = \int \pi(\boldsymbol{\phi}_s, \sigma_s^2 | T, x) d\sigma_s^2 \propto \int \left(\frac{1}{\sigma_s^2} \right)^{\tilde{\tau}+1} \exp \left(- \frac{L}{2\sigma_s^2} \right) d\sigma_s^2 = \frac{\Gamma(\tilde{\tau})}{(L/2)^{\tilde{\tau}}}.$$

So, as a function of $\boldsymbol{\phi}_s$, the posterior $\pi(\boldsymbol{\phi}_s | T, x)$ is,

$$\begin{aligned} \pi(\boldsymbol{\phi}_s | T, x) &\propto L^{-\tilde{\tau}} = \left(2\lambda + D_s + (\boldsymbol{\phi}_s - \mathbf{m}_s)^T (S_3 + \Sigma_o^{-1}) (\boldsymbol{\phi}_s - \mathbf{m}_s) \right)^{-\frac{2\tau+|B_s|+p}{2}} \\ &\propto \left(1 + \frac{1}{2\tau + |B_s|} (\boldsymbol{\phi}_s - \mathbf{m}_s)^T \frac{(S_3 + \Sigma_o^{-1})(2\tau + |B_s|)}{(2\lambda + D_s)} (\boldsymbol{\phi}_s - \mathbf{m}_s) \right)^{-\frac{2\tau+|B_s|+p}{2}} \\ &\propto \left(1 + \frac{1}{\nu} (\boldsymbol{\phi}_s - \mathbf{m}_s)^T P_s^{-1} (\boldsymbol{\phi}_s - \mathbf{m}_s) \right)^{-\frac{\nu+p}{2}}, \end{aligned}$$

which is exactly in the form of a multivariate t -distribution, with p being the dimension of $\boldsymbol{\phi}_s$, and with ν , \mathbf{m}_s and P_s exactly as given in Lemma 2, completing the proof. \square

C List of datasets

C.1 sim_1

The dataset `sim_1` is a simulated dataset, which consists of $n = 600$ observations generated from a BCT-AR model with the tree model of Figure 1, quantiser threshold $c = 0$, and AR order $p = 2$. The complete specification of this BCT-AR model, is also given in the main text,

$$x_n = \begin{cases} 0.7 x_{n-1} - 0.3 x_{n-2} + e_n, & e_n \sim \mathcal{N}(0, 0.15), & \text{if } s = 1: x_{n-1} > 0, \\ -0.3 x_{n-1} - 0.2 x_{n-2} + e_n, & e_n \sim \mathcal{N}(0, 0.10), & \text{if } s = 01: x_{n-1} \leq 0, x_{n-2} > 0, \\ 0.5 x_{n-1} + e_n, & e_n \sim \mathcal{N}(0, 0.05), & \text{if } s = 00: x_{n-1} \leq 0, x_{n-2} \leq 0. \end{cases}$$

Here, we also report the *evidence* $p(x|c, p)$ for a range of values of c and p . Although maximising the evidence is a very common, well-justified Bayesian practice [60, 48, 61], here we report some values as a sanity check, to show that the evidence is indeed maximised at the true values of $c = 0.0$ and $p = 2$, and thus verify in practice that our inferential procedure for choosing c and p is effective.

Table 2: Using the evidence $p(x|c, p)$ to choose the AR order and the quantiser threshold

	AR order p					Threshold c				
	1	2	3	4	5	-0.1	-0.05	0	0.05	0.1
$-\log_2 p(x c, p)$	533	519	526	531	535	558	539	519	555	577

C.2 sim_2

The dataset `sim_2` is a simulated dataset, which consists of $n = 500$ observations generated from a BCT-AR model with respect to the ternary tree in Figure 4. The thresholds of the quantiser are $\{c_1 = -0.5, c_2 = 0.5\}$, and the AR order is $p = 1$. The complete specification of this BCT-AR model, is given by,

$$x_n = \begin{cases} 0.5 e_n, & \text{if } s = 1, 01, 02, 20, 21, \\ 0.99 x_{n-1} + 0.005 e_n, & \text{if } s = 00, 22, \end{cases}$$

with $e_n \sim \mathcal{N}(0, 1)$.

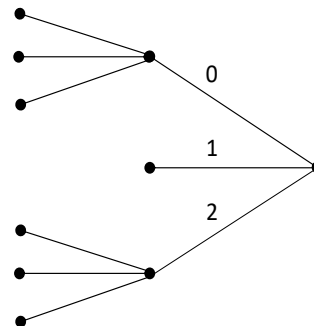


Figure 4: Tree model of `sim_2`

C.3 sim_3

The dataset `sim_3` is a simulated dataset, which consists of $n = 150$ observations generated from a SETAR model of order $p = 1$, given by,

$$x_n = \begin{cases} -0.25 + 0.9 x_{n-1} + 0.5 e_n, & \text{if } x_{n-1} > 0.15, \\ 0.15 - 0.8 x_{n-1} + 0.2 e_n, & \text{if } x_{n-1} \leq 0.15, \end{cases}$$

where here, as it is common practice, for simplicity we include the noise variance in the coefficients of e_n , so that $e_n \sim \mathcal{N}(0, 1)$.

C.4 sim_4

The dataset `sim_4` is a simulated dataset, which consists of $n = 200$ observations generated from a SETAR model of order $p = 5$, given by,

$$x_n = \begin{cases} -0.1 + 0.9 x_{n-1} + 0.9 x_{n-2} - 0.2 x_{n-5} + e_n, & \text{if } x_{n-1} > -0.2, \\ 0.2 + 0.1 x_{n-1} + 0.9 x_{n-5} + e_n, & \text{if } x_{n-1} \leq -0.2, \end{cases}$$

with $e_n \sim \mathcal{N}(0, 1)$.

C.5 unemp

The dataset `unemp` is a real dataset, which consists of $n = 288$ observations of the quarterly US unemployment rate in the time period from 1948 to 2019. It is publicly available from the US Bureau of Labor Statistics (BLS), at https://data.bls.gov/timeseries/LNS14000000?years_option=all_years.

C.6 gnp

The dataset `gnp` is a real dataset, which consists of $n = 291$ observations of the quarterly US Gross National Product (GNP) in the time period from 1947 to 2019. It is available from the US Bureau of Economic Analysis (BEA), and can be retrieved from the Federal Reserve Bank of St. Louis (FRED) at <https://fred.stlouisfed.org/series/GNP>.

For this dataset, the MAP BCT tree model is given in the main text, in Figure 2: It has depth $d = 3$, four leaves $\{0, 10, 110, 111\}$, and posterior 42.6%. The threshold of the binary quantiser selected using the procedure of Section 3.2 is $c = 0.2$, so that $s = 1$ if $y_{n-1} > 0.2$ and $s = 0$ if $y_{n-1} \leq 0.2$. The AR order selected is $p = 2$. The complete BCT-AR model, with its MAP estimated parameters is given by,

$$y_n = \begin{cases} 1.156 + 0.714 y_{n-1} + 0.186 y_{n-2} + 1.23 e_n, & \text{if } s = 0, \\ 0.177 + 0.679 y_{n-1} - 0.260 y_{n-2} + 1.19 e_n & \text{if } s = 10, \\ -1.054 + 1.403 y_{n-1} + 0.194 y_{n-2} + 1.04 e_n & \text{if } s = 110, \\ 0.593 + 0.281 y_{n-1} + 0.305 y_{n-2} + 0.75 e_n & \text{if } s = 111, \end{cases}$$

with $e_n \sim \mathcal{N}(0, 1)$.

C.7 ibm

The dataset `ibm` is a real dataset, which consists of $n = 369$ observations of the daily IBM common stock closing price, in the time period from May 17, 1961 to November 2, 1962. The dataset is taken from [10], and it is also available from the R package `fma` [34]. The MAP tree model fitted to the dataset is shown in the main text at Figure 3. The complete BCT-AR model, with its MAP estimated parameters, is given by,

$$x_n = \begin{cases} 1.03 x_{n-1} - 0.03 x_{n-2} + 12.3 e_n, & \text{if } s = 0, \\ 1.17 x_{n-1} - 0.17 x_{n-2} + 6.86 e_n, & \text{if } s = 2, \\ -0.11 x_{n-1} + 1.11 x_{n-2} + 10.8 e_n, & \text{if } s = 10, \\ 1.22 x_{n-1} - 0.22 x_{n-2} + 5.32 e_n, & \text{if } s = 11, \\ 0.15 x_{n-1} + 0.85 x_{n-2} + 5.17 e_n, & \text{if } s = 12, \end{cases}$$

with $e_n \sim \mathcal{N}(0, 1)$.

Multi-step ahead forecasting. As explained in the main text, in this example many approaches were found to have similar prediction performance when considering 1-step ahead forecasts. For this reason, we perform more extensive comparisons, and also consider multi-step ahead forecasts (2-step and 3-step). For multi-step-ahead forecasts, we use the parametric bootstrap of [76, p. 192]: We sample trajectories from the model, and use the sample average as the point forecast. From the results of Table 3, it is observed that even though deepAR has the best performance in 1-step ahead forecasts, its performance quickly deteriorates with larger prediction horizons, and BCT-AR has the best performance in the multi-step ahead forecasts (both 2-step and 3-step).

Table 3: Mean squared error (MSE) of multi-step ahead forecasts in the `ibm` dataset

	BCT-AR	ARIMA	ETS	NNAR	deepAR	N-BEATS	GP	SETAR	MAR
1-step	78.02	82.90	77.52	78.90	75.71	77.90	87.27	81.07	77.02
2-step	75.72	79.20	77.99	75.92	83.74	75.78	87.16	78.68	76.49
3-step	75.79	78.42	77.57	76.21	83.87	78.55	85.32	78.64	76.58

D Training details

Here we specify the training details for all the methods used in the forecasting experiments. In all the examples the training set consists of the first 50% of the observations, and we allow updates at every timestep for all methods. From the R package `forecast` [35], the functions `auto.arima` and `ets` for fitting the ARIMA and ETS models are completely automated, so there are no parameters to specify here. For NNAR, we use the function `nnetar` which is also contained in the `forecast` package, and search over AR orders between $p = 1$ and $p = 5$. For the BCT-AR model, we choose the AR order and the quantiser thresholds at the end of the training set, and then use the MAP tree model and parameters updated at every timestep, as explained in detail in the main text.

For deepAR, N-BEATS, and GP, we use the implementations in the Python library GluonTS [3]. As the computational cost per iteration differs for these methods, we use slightly different numbers of epochs and batches-per-epoch for each of them, in order to give similar empirical running times – which are still much higher than those of our methods; see below. For deepAR we use 5 epochs with 50 batches/epoch, for GP we use 10 epochs with 100 batches/epoch, and for N-BEATS we use 3 epochs with 20 batches/epoch. In all cases we try AR orders between $p = 1$ and $p = 5$. For the SETAR model, we use the R package `TSA` [13], along with the commonly used conditional least squares method of [12]. We search over AR orders between $p = 1$ and $p = 5$, and values of the delay parameter between $d = 1$ and $d = 5$. For the MAR model, we use the R package `mix-AR` [9], and try $K = 2$ and $K = 3$ components with AR orders between $p = 1$ and $p = 5$.

E Empirical running times

As discussed in Section 3.1, an important advantage of the BCT-AR framework is that the associated algorithms allow for very efficient sequential updates, making it very practical for online forecasting applications. This is in sharp contrast with deepAR, N-BEATS, and GP,

whose current implementation in GluonTS does not allow for incremental training, so the models are re-trained in each timestep from scratch; something which is computationally very costly. The classical statistical approaches lie somewhere in-between the two extremes, as they are re-trained at every timestep using the `forecast` package, but the cost required per timestep is lower than that of the ML methods; see also [50]. From Table 4 it is observed that, because of its efficient sequential updates, BCT-AR clearly outperforms all the benchmarks in terms of empirical running times. The only method achieving somewhat comparable performance is ETS, but BCT-AR was found to perform much better in terms of MSE. All experiments were carried out on a common laptop.

Table 4: Empirical running times*

	BCT-AR	ARIMA	ETS	NNAR	deepAR	N-BEATS	GP	SETAR	MAR
<code>sim_1</code>	7.4 s	1.1 min	31 s	4.9 min	2.4 h	7.4 h	5.2 h	1.3 min	19 min
<code>sim_2</code>	8.1 s	1.0 min	23 s	3.2 min	2.1 h	6.3 h	4.3 h	2.0 min	2.5 min
<code>sim_3</code>	1.6 s	22 s	3.2 s	9.3 s	36 min	2.5 h	1.1 h	5.2 s	2.2 min
<code>sim_4</code>	2.4 s	28 s	5.2 s	48 s	55 min	4.0 h	2.2 h	11 s	2.7 min
<code>unemp</code>	3.1 s	42 s	11 s	1.2 min	59 min	4.1 h	1.6 h	17 s	6.4 min
<code>gnp</code>	2.2 s	1.3 min	10 s	1.5 min	1.5 h	5.2 h	2.0 h	19 s	6.6 min
<code>ibm</code>	4.6 s	58 s	16 s	32 s	2.2 h	5.3 h	3.6 h	28 s	7.6 min

*The empirical running times of deepAR, N-BEATS and GP could be greatly reduced if the model was not updated at every timestep. In this case, the difference from BCT-AR would not be so substantial. Nonetheless, even the fact that gradient optimisation is needed (involving a significant number of iterations) makes their training per-timestep much more computationally expensive compared to BCT-AR; see also the review [50] discussing the computational requirements of recent ML methods in time series forecasting.